engineering proceedings

MDPI

*Proceeding Paper*

# Survivability Approach to Increase the Resilience of Critical Systems †

**Salvatore Annunziata *, Luca Lomazzi, Marco Giglio and Andrea Manes**

Departement of Mechanical Engineering, Politecnico di Milano, Via Giuseppe La Masa 1, 20156 Milan, Italy; luca.lomazzi@polimi.it (L.L.); marco.giglio@polimi.it (M.G.); andrea.manes@polimi.it (A.M.)

* Correspondence: salvatore.annunziata@polimi.it

† Presented at the 53rd Conference of the Italian Scientific Society of Mechanical Engineering Design (AIAS 2024), Naples, Italy, 4–7 September 2024.

**Abstract:** The survivability approach necessitates a vulnerability assessment, which quantifies the likelihood that a platform will be rendered inoperative when exposed to a threat—whether man-made or natural. This concept is closely tied to survivability, defined as the probability that a platform will complete its assigned mission. Detection and potential exposure to a threat can significantly reduce a system's survivability. As a result, vulnerability evaluation has become a critical aspect of designing platforms that operate in high-risk environments. Numerous techniques have been developed for vulnerability assessment, with many studies aimed at achieving increasingly accurate evaluations to improve the reliability and safety of mechanical systems. Notably, in 1985, Ball introduced the concept of survivability, outlining various design solutions and techniques for fixed-wing and rotary-wing aircraft. Since then, several vulnerability assessment programs have been launched, leading to the creation of some of the most resilient platforms in use today. The assessment of vulnerability plays a key role in determining solutions to enhance the likelihood of a system successfully completing its mission. In this context, this paper presents the application of in-house software to analyze a fixed-wing Remotely Piloted Aircraft System (RPAS). The model used to validate the software's capabilities was developed using publicly available data, enabling a practical demonstration of the software's functionality. Applied to this case study, the software assesses the RPAS vulnerability against various impact threats. The software not only evaluates vulnerability but also suggests protective solutions to mitigate it. This application demonstrates how the software can enhance the reliability and safety of an existing operational system while also showcasing its potential for use during the preliminary design phase of a broader range of platforms.

**Keywords:** vulnerability; protective structures; impacting objects; fragments; topology optimization; case study; weight estimation



Academic Editors: Umberto Galietti, Gabriele Arcidiacono, Enrico Armentani, Davide Castagnetti, Vigilio Fontanari, Aurelio Somà and Nicola Bonora

Published: 19 February 2025

**Citation:** Annunziata, S.; Lomazzi, L.; Giglio, M.; Manes, A. Survivability Approach to Increase the Resilience of Critical Systems. *Eng. Proc.* **2025**, *85*, 22. https://doi.org/10.3390/engproc2025085022



## 1. Introduction

The ability of a platform to withstand or evade hostile threats is a cornerstone of modern vehicle design, particularly in aerospace and defense applications. Survivability, defined as the capability of a platform to continue its mission despite damage or threat exposure, relies on reducing two key factors: susceptibility and vulnerability. While susceptibility refers to a platform's likelihood of being detected, targeted, and hit, vulnerability is concerned with the platform's ability to withstand those hits once they occur [1]. In recent years, significant strides have been made in designing platforms that not only avoid detec-

tion but also integrate protective systems to mitigate damage from threats like impacting objects and fragments.

The early work in survivability can be traced back to World War I, where basic protective measures were introduced to improve the resilience of aircraft [1]. This discipline evolved considerably through the subsequent conflicts, especially during the Cold War, where high-threat environments necessitated the development of platforms with enhanced vulnerability reduction measures [2,3]. By the 1980s, the importance of survivability in both military and civilian platforms led to the establishment of dedicated survivability centers, such as the Department of Defense's Survivability/Vulnerability Information Analysis Center (SURVIAC) [1,4].

Most of the existing research on vulnerability and survivability has focused on creating assessment tools to analyze how platforms perform under hostile conditions. Vulnerability analysis typically involves identifying the critical components of a platform that, if damaged, could affect its functionality. To support these assessments, computational tools such as FASTGEN and COVART were developed to simulate impact scenarios and evaluate how different elements of the platform contribute to its overall vulnerability [5,6]. These tools rely on ray-tracing algorithms and statistical frameworks to calculate the probability of critical damage from threats like projectiles or missile fragments [7].

While survivability and vulnerability concepts were first formalized in the aeronautical sector, their applications have since expanded into other fields, including naval and ground combat systems. For instance, Kincheloe et al. [8] developed vulnerability models for ground combat systems, and Yoo and Park [9] extended these concepts to ground vehicles using fault tree analyses. In naval contexts, recent studies have developed vulnerability assessment models to evaluate early-stage warship design [10].

Despite the availability of sophisticated vulnerability analysis methods, efforts to reduce vulnerability often face a critical challenge: the trade-off between adding protective structures and maintaining platform performance. Particularly in aerospace applications, where weight is a critical factor, increasing structural weight to accommodate protective measures can adversely affect fuel efficiency, maneuverability, and mission endurance. Therefore, one of the primary goals in modern platform design is to optimize protective structures to minimize weight while ensuring maximum survivability.

Topological optimization has emerged as a powerful tool for addressing this challenge. By optimizing the layout of protective materials, engineers can develop solutions that protect critical components without excessive weight gain. Techniques such as genetic algorithms (GAs) [11–13], solid isotropic material with penalization (SIMP) [14,15], and evolutionary structural optimization (ESO) [16,17] have been successfully applied in various structural optimization problems. Among these methods, multi-objective genetic algorithms are particularly promising because they enable designers to balance competing objectives, such as minimizing weight and vulnerability.

In the context of vulnerability-driven design, recent work by Lomazzi et al. [18] and Annunziata et al. [19] has demonstrated how multi-objective genetic algorithms can be employed to optimize protective structures against impacting objects and fragments. These studies introduced a probabilistic approach to vulnerability analysis, integrating ray-tracing techniques with genetic algorithms to optimize protective solutions in real-world scenarios. The novelty of these approaches lies in their ability to generate non-dominated solutions that balance protection and weight, enabling designers to choose the optimal configuration based on mission-specific requirements.

Building on these advancements, this work presents an application of the developed integrated framework for the topological optimization of protective structures. Leveraging in-house vulnerability analysis software, the proposed method employs genetic algorithms

to generate protective designs that mitigate vulnerability while maintaining minimal weight increases. By focusing on two distinct types of impacts, the framework aims to provide a versatile solution for various platform design challenges. Through a representative case study involving a platform subjected to both impacting objects and fragments, the effectiveness of this optimization tool in improving survivability without compromising structural performance is demonstrated.

This paper is organized as follows: Section 2 provides a brief overview of the developed algorithms. Since the primary focus of this work is to demonstrate the application of these algorithms to a complex and realistic case study, the algorithm descriptions are intentionally concise. Readers interested in a more detailed explanation are encouraged to refer to Refs. [18,19]. In Section 3, the platform used for the case study is described in detail, including how its components were modeled and the results obtained. These results cover the platform's vulnerability assessment, the optimized protective structures, and an estimation of the weight of the protective solutions. Finally, Sections 4 and 5 present a critical discussion of the findings, followed by the conclusions drawn from this study.

## 2. Materials and Methods

In the integrated computational environment, two modules have been developed for the generation and topological optimization of protective structures, each specialized for a specific threat of interest. The module handling impacting objects defines the topology of flat, non-curved protection, earning the name 2D algorithm. On the other hand, the algorithm developed for fragments enables the design of protection in three-dimensional space and is therefore referred to as the 3D algorithm. The following subsections provide a description of the algorithms developed. However, before proceeding with the generation and optimization of the protective structures, it is essential to first assess the vulnerability of the unprotected platform. This assessment, carried out for both the 2D and 3D algorithms, is crucial for identifying critical components that require protection and for gathering all necessary data to achieve topologically optimized defenses. The functioning of these two modules is explored in more detail in Sections 2.1 and 2.2.

### *2.1. Vulnerability Assessment and Protection Topology Optimization: Impacting Objects*

This paragraph provides a general overview of the code related to protections against impacting objects. For interested readers, the part of the code related to the vulnerability assessment is detailed in Ref. [18], while the part dedicated to the generation and optimization of the protective structure is reported in Ref. [19]. Here, a general description is provided to better appreciate the results obtained through the application of the algorithm to the case study. Specifically, the 2D algorithm is structured as shown in Figure 1 and follows these phases:

1. Initial vulnerability assessment of the unprotected platform. This phase involves conducting a vulnerability analysis aimed at identifying the critical component that requires protection. In case of a multi-hit scenario, a Monte Carlo analysis is necessary.
2. Protection initialization. Once the critical component and the area of interest have been identified, the protection's topology is initialized. The grid from which the shot-lines originate is used for the generation of the protection too. At this stage, the protection is discontinuous and blocks all threat trajectories that would intercept the component.
3. Optimization. The protection's topology is optimized using a multi-objective genetic algorithm, which aims to simultaneously minimize both the solution's weight and the vulnerability of the critical component.

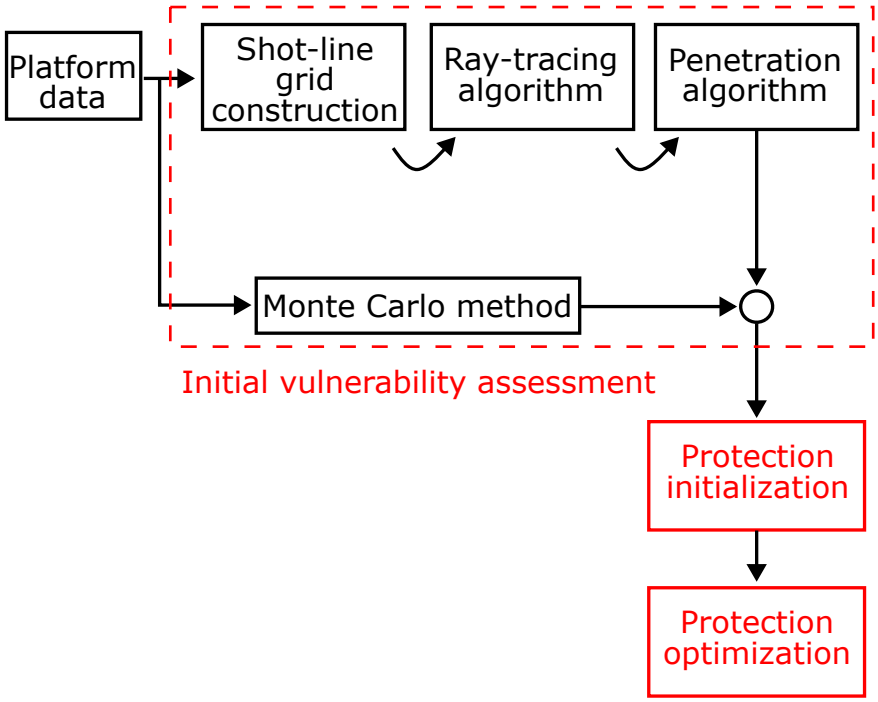


**Figure 1.** Vulnerability and protection generation with respect to impacting objects: 2D algorithm workflow.

The inputs and outputs obtained after the optimization process are described in the following sections.

#### 2.1.1. Inputs

The 2D algorithm requires both inputs related to the vulnerability assessment of the structure against impacting objects and inputs specific to the optimizer.

The inputs related to the vulnerability assessment include the data reported in Table 1.

**Table 1.** Inputs related to the 2D algorithm.

| Input Data | Description |
|---|---|
| N | Number of simultaneous impacting objects |
| Diameter | Dimensions of the impacting objects |
| Velocity | Impact velocity |
| Resolution | Grid resolution |
| Aspect | Azimuth and Elevation angles defining threat direction |

The code is able to assess the vulnerability of the target platform considering one or multiple impacting objects. Moreover, increasing the resolution of the grid affects the dimensions of the square cells composing it. Thus, the number of trajectories increases too, improving the reliability of the vulnerability assessment. In addition to the quantitative inputs listed in the table, for the correct operation of the code, it is necessary to provide the target platform model and a text file containing the names of the critical components, the systems they belong to, the material they are composed of, and the probability that they will be rendered inoperative when hit by an object.

The inputs for the optimization phase are as follows:

- The critical component to be protected;
- The nature of the design variables;
- The population size for the optimization process;
- The initial population;

- Optimization tolerance;
- Maximum number of iterations;
- Crossover function and fraction;
- Mutation function.

The critical component to be protected is identified through the initial vulnerability analysis conducted without considering the presence of protective materials. The design variables are discrete and can take a value of either 0 or 1, where 0 indicates the absence of protective material and 1 indicates its presence. In the case of the 2D algorithm, the initial population consists of identical individuals, all characterized by the presence of protective material along the trajectories that intersect the target critical component.

#### 2.1.2. Outputs

The outputs of the code consist of graphs that display the vulnerability values of the platform, as well as the systems and components it comprises, based on the aspects considered in the analysis. Regarding the generation of protective structures, the outputs include a set of optimal protections. This set represents the solutions on the Pareto front, a collection of dominant solutions identified by the genetic algorithm.

### *2.2. Vulnerability Assessment and Protection Topology Optimization: Fragments*

The code for optimizing protection against fragments is independent of the one described in Section 2.1, and it utilizes an updated version of the ray-tracing algorithm initially developed for impacting objects. This paragraph provides a general overview of the code related to protections against fragments. For interested readers, the part of the code related to vulnerability assessment and protection generation and optimization is detailed in Ref. [19]. Here, a general description is provided to better appreciate the results obtained through the application of the algorithm to the case study.

Specifically, the software dedicated to fragment-based protection generation and optimization presents the workflow shown in Figure 2.

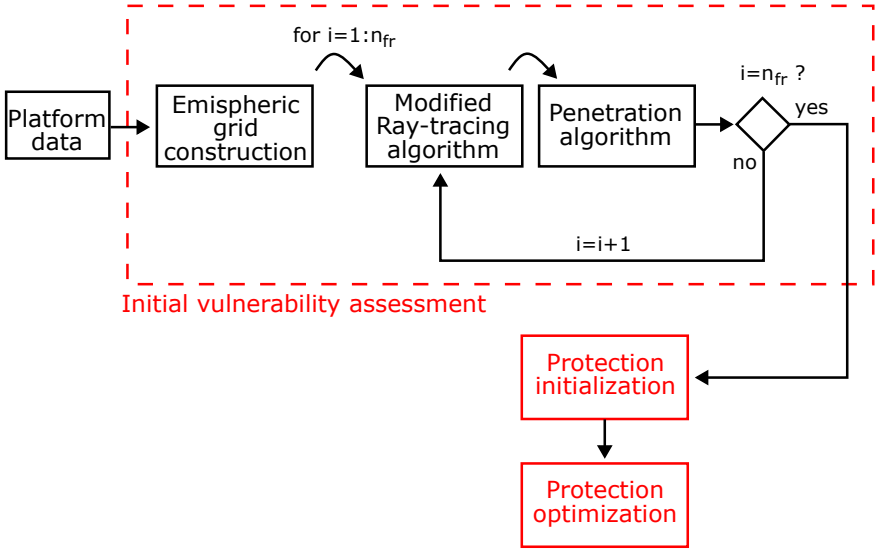


**Figure 2.** Vulnerability and protection generation with respect to fragments: 3D algorithm workflow.

The procedure consists of the following phases:

1. Initial vulnerability assessment of the unprotected platform. This phase involves conducting a vulnerability analysis to identify the critical component that requires protection.

2. Initialization of the protection. After identifying the critical component, the protection topology is initialized. At this stage, the protection is discontinuous and blocks all threat trajectories that would intersect the component.
3. Optimization. The protection topology is optimized using a multi-objective genetic algorithm to simultaneously minimize the solution's weight and the critical component's vulnerability.

The following sections will describe the inputs required for the software to begin the analysis and the outputs generated by the developed process.

#### 2.2.1. Inputs

The 3D algorithm requires inputs related to the characteristics of the detonating object to generate the trajectories and assess vulnerability. These inputs are listed and briefly described in Table 2. The susceptibility of the i-th component $P_{hi}$ is defined as the probability that the platform is detected and hit. The azimuth and elevation angles associated with the detonating object describe its targeting orientation, thus indicating the direction of movement toward the target. The vulnerability assessment is generally conducted by considering multiple detonation distances of interest. The module requires specifying the range of detonation distances [$DD_{min}$ $DD_{max}$] for which the vulnerability assessment is to be performed and the number of distances $N_{DD}$ within that range, including the boundaries. Based on these values, $N_{DD}$ distances are selected at regular intervals within the previously defined range. For each detonation distance considered in the assessment, a hemispherical detonation grid is generated. Each grid has a radius equal to the related detonation distance. The number of detonation points per grid is defined by parameters $N_{DP,xy}$ and $N_{DP,xz}$.

**Table 2.** Inputs related to the 3D algorithm.

| Input Data | Description |
|---|---|
| $V_m$ | Speed of the detonating object originating the fragments |
| $Az_m$ | Azimuth angle of the detonating object |
| $El_m$ | Elevation angle of the detonating object |
| $DD_{min}$ | Minimum value of the detonation distance interval |
| $DD_{max}$ | Maximum value of the detonation distance interval |
| $N_{DD}$ | Number of detonation distances |
| $N_{DP,xy}$ | Number of detonation points on the $x$–$y$ plane |
| $N_{DP,xz}$ | Number of detonation points on the $x$–$z$ plane |
| $P_{hi}$ | Susceptibility of the $i$-th component |
| $Height$ | Altitude of the detonation point |
| $L_{wh}$ | Detonation object length |
| $D_{wh}$ | Detonation object diameter |
| $h_{wh}$ | Detonation object case thickness |
| $A_f$ | Area of the fragment |
| $m_f$ | Mass of the fragment |

Additionally, the algorithm requires inputs related to the optimizer, specifically the same ones already mentioned in Section 2.1 for the 2D algorithm.

#### 2.2.2. Outputs

The outputs of the code consist of vulnerability and detonation distance graphs for each component, system, and the entire platform. The outputs of the optimization process consist of a set of optimal protections. This set represents the solutions on the Pareto front, which is the collection of dominant solutions identified by the genetic algorithm. These

solutions achieve a balance between minimizing the weight of the protection and reducing the vulnerability of the critical component.

2.2.3. Evaluation of Protection's Weight

To provide a quantitative benchmark for the topological optimization of protective structures with respect to fragments, it is possible to evaluate the thickness and, consequently, the weight of the generated solutions. This can be achieved using analytical methods based on a specific equation that describes the ballistic limit velocity ($V_{bl}$). The ballistic velocity depends on the areal density of the fragment ($AD_p$) and the target ($AD_t$). In the following paragraphs, by applying the code to a specific case study, the weight of the protective structure will be estimated under the assumption that it has a thickness that is sufficient to completely stop the penetration of the threat, and that the material composing the protection is Dyneema HB26.

## 3. Results

### *3.1. Case Study*

The codes described in the previous sections were applied to a sufficiently complex case study to test the performance of the developed framework and verify the quality of the results.

The demonstrator selected for the vulnerability analysis and protection generation is Predator RQ-1. This was undertaken because a wide range of publicly available data exist for this platform, which enables accurate modeling. The main dimensions of the Predator RQ-1 RPAS are shown in Figure 3.

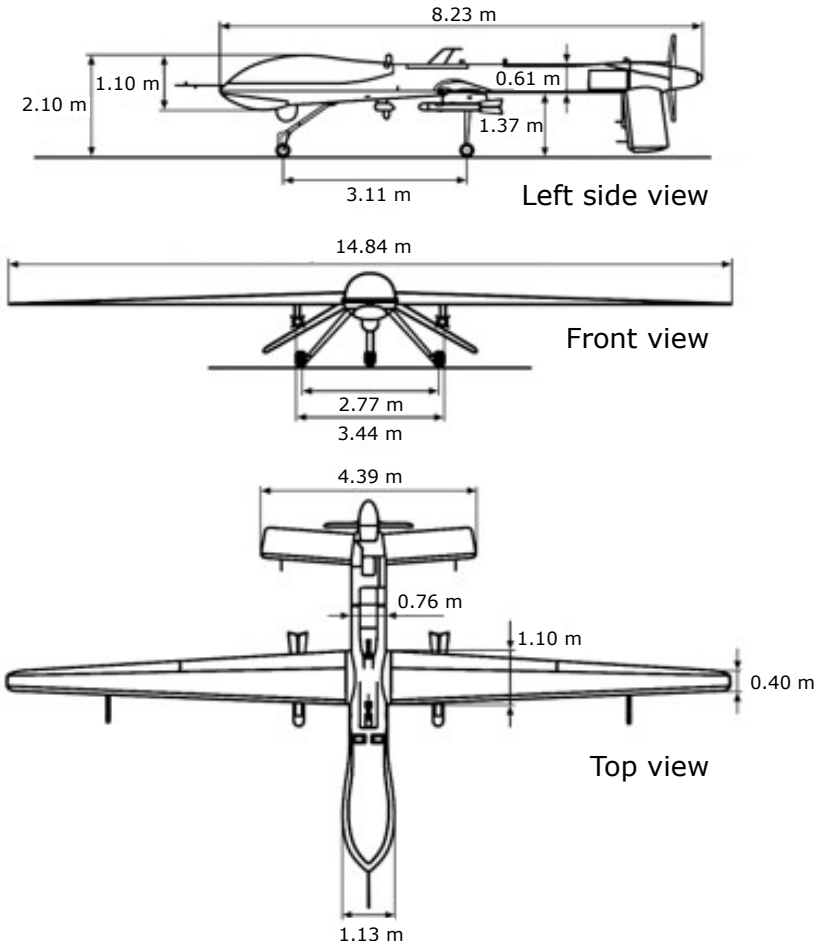


**Figure 3.** Characteristic dimensions of RQ−1 presented as a case study.

Due to its relatively small thickness, the platform's fuselage has negligible effects on fragments and impacting objects during penetration. As a result, the velocity of a threat after passing through the fuselage is assumed to be the same as its velocity just before the impact.

Each element of the platform must be modeled simplifying its shape before compiling the model input file. The process for determining the thicknesses of the simplified shapes for RQ-1's components is described in the following section.

Component's Modeling

Simplifying the shapes of the components is essential to permit their representation through the composition of simple shapes: triangles. This type of representation is used because it accurately describes the component while keeping the file sizes relatively small, reducing the computational cost without affecting the quality of the analyses. To effectively reduce the time required for the software to perform all the calculations, the components involved in the vulnerability assessment need to be simplified, preserving the same volume and mass as the original object. This is achieved by designing simple hollow shapes with wall thicknesses that meet these requirements. The simplification process is carried out in two steps: the first involves modeling the box so that it encloses the original object, ensuring that the volume (or presented area) is preserved. Next, the wall thickness $t$ is determined to meet the requirement of mass preservation.

Considering a box like the one shown in Figure 4, the equations to find the thickness $t$ are provided in Equations (1)–(3), where $M$ is the mass of the object, $\rho$ is the density of the material the component is composed of, $V$ is the volume of the object, and $a$, $b$, and $c$ are the dimensions of the cuboid, while $t$ represents the wall thickness.

$$M_{original} = M_{simplified} \tag{1}$$

$$M_{original} = \rho_{simplified} \cdot V_{simplified} \tag{2}$$

$$M_{original} = \rho_{simplified} \cdot [a \cdot b \cdot c - (a - 2t) \cdot (b - 2t) \cdot (c - 2t)] \tag{3}$$

By solving Equation (3) for $t$, the wall thickness of the cuboid can be determined to ensure that the mass is preserved while maintaining the same volume. These thicknesses enable the estimation of threat deceleration upon the penetration of the components. This process must be repeated for each component of the platform included in the analysis. In Table 3, the data and the computed thicknesses for all the critical components are reported.

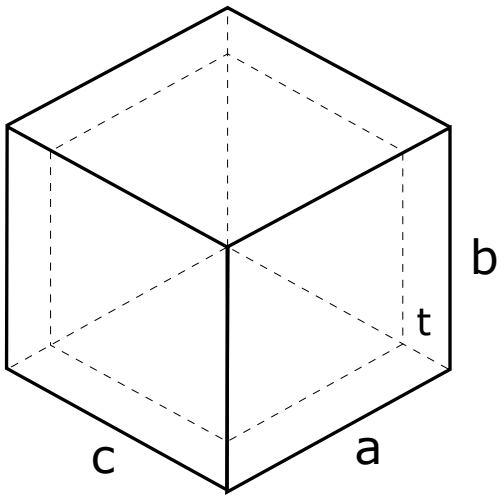


**Figure 4.** Representative simplified geometry of a platform component.

**Table 3.** Platform's critical components' dimensions and equivalent thicknesses.

| Components | Dimensions [mm] | Material | Box Thickness |
|---|---|---|---|
| Inertial navigation system/global position system | 120 × 200 × 70 | Aluminum | $t = 6.4$ mm |
| Forward fuel tank | 490 × 450 × 1221 | Kevlar | $t = 5$ mm |
| Aft fuel tank | 490 × 450 × 1221 | Kevlar | $t = 5$ mm |
| Airborne VCR | 114 × 212 × 345 | Aluminum | $t = 10$ mm |
| GPS antenna (left and right) | 128 × 86 × 256 | Aluminum | $t = 6.7$ mm |
| Nose camera | 43 × 44 × 62.4 | Aluminum | $t = 3.1$ mm |
| Payload and power distribution panel | 193 × 121 × 36.2 | Aluminum | $t = 3.3$ mm |
| Nose blanket heating controller | 60 × 45 × 31 | Aluminum | $t = 3.5$ mm |
| Tail servo (left and right) | 45 × 118.3 × 159 | Aluminum | $t = 14.4$ mm |
| Battery 1 | 135 × 223 × 182 | Aluminum | $t = 11$ mm |
| Battery 2 | 135 × 223 × 182 | Aluminum | $t = 11$ mm |
| Aft batteries (left and right) | 135 × 223 × 182 | Aluminum | $t = 11$ mm |
| Dual alternator regulator | 55 × 96 × 160 | Aluminum | $t = 3.8$ mm |
| Battery charger contactors | 89 × 133 × 127 | Aluminum | $t = 13.7$ mm |
| Engine | 1022.1 × 450 × 300 | Steel | $t = 4.2$ mm |
| Oil cooler/radiator | 228 × 147 × 51 | Aluminum | $t = 3.6$ mm |

Using the text file composed of the simplified components, it is possible to obtain the platform representation shown in Figure 5.

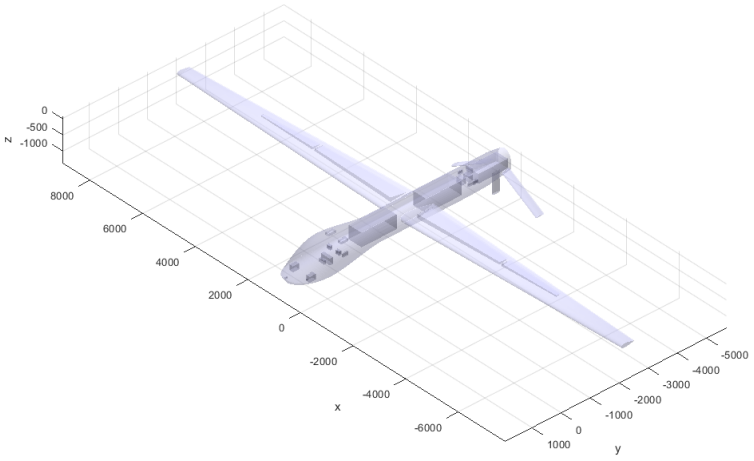


**Figure 5.** RQ−1 simplified model used as the target platform.

### *3.2. Vulnerability Assessment and Protective Structures Against Impacting Objects*

With the input values reported in Table 4, the algorithm calculates the vulnerability of the platform, the systems, and the components that comprise it.

**Table 4.** Inputs related to the 2D algorithm, specific to the considered case study.

| Input data | Description | Values |
|---|---|---|
| N | Number of simultaneous impacting objects | 4 |
| Diameter | Dimensions of the impacting objects | 12.7 mm |
| Velocity | Impact velocity | 487 m/s |
| Resolution | Grid resolution | 50 mm |
| Aspect | Azimuth and Elevation angles | $[0°; -40°]$ $[-40°; +40°]$ |

In Figure 6a,b, the vulnerability values of the platform and a component, respectively, are shown with respect to the considered aspects. From this analysis, the software identifies

the aspect characterized by azimuth and elevation angles equal to 0° and the component Airborne-VCR as the most critical. Consequently, it generates an optimized protective system for this component. The optimization module for impacting objects, therefore, converges to the solution shown in Figure 7.

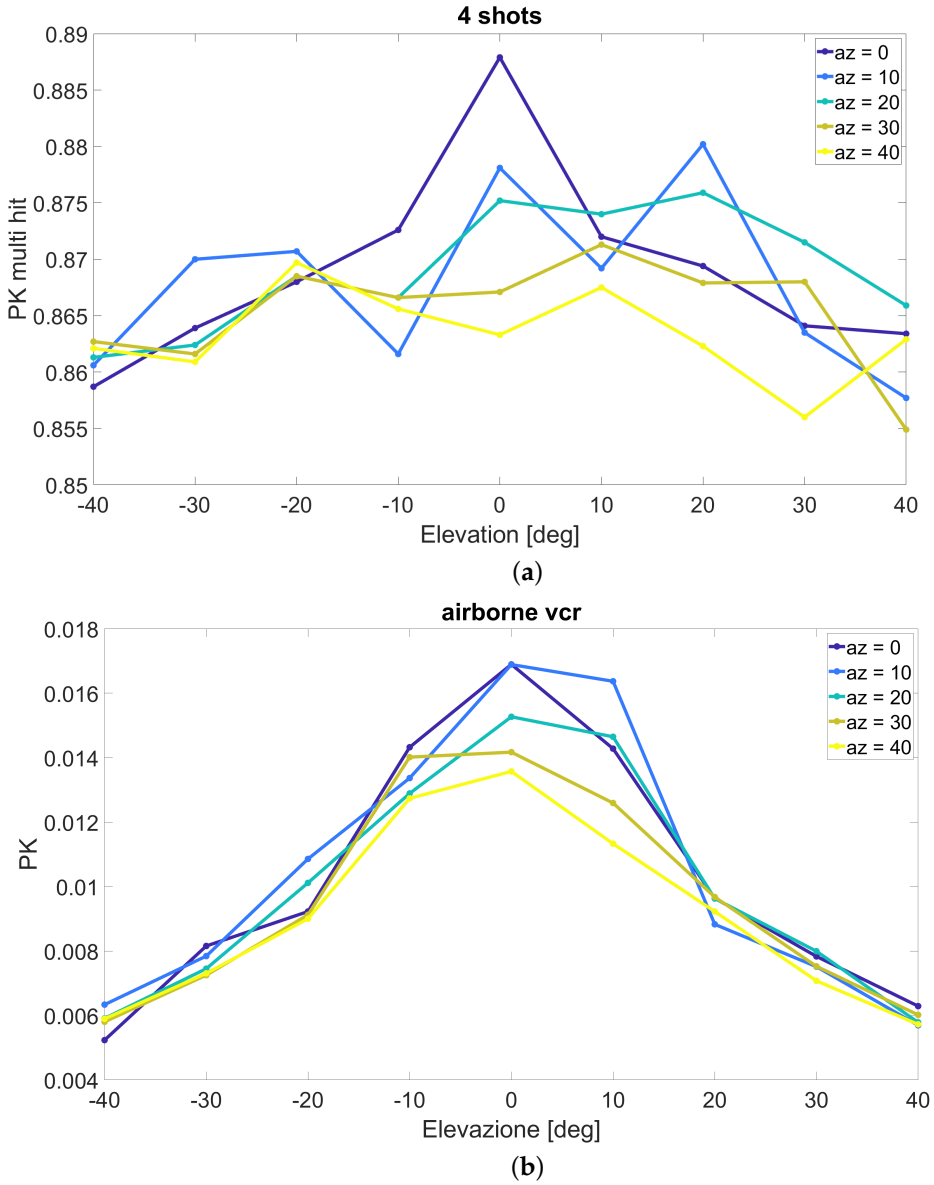


**Figure 6.** Vulnerability assessment of the entire platform (**a**) and of the most critical components (**b**) considering multiple shots and multiple aspects.

Here, the red dots are the representation of the solution at which the algorithm converges. In the Pareto front, not reported here because it is composed of a single point, the solution is represented as a point in the weight–vulnerability ($P_k$) graph, with coordinates $(0.0028; 0)$. The weight of the protection is normalized with respect to the total number of cells in the optimization grid. The module converges to a single solution, eliminating the vulnerability. To reduce the component's vulnerability to zero, the algorithm places protective elements in all the elements from which shot-lines impacting the component originate, effectively covering its projection relative to the considered aspect.

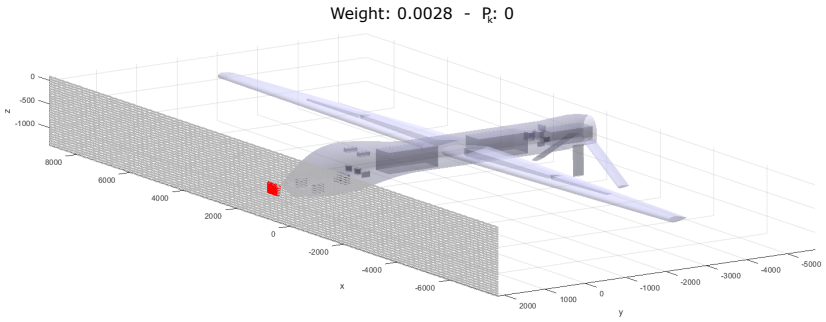


**Figure 7.** Visualization of the optimized protection against impacting objects.

### *3.3. Vulnerability Assessment and Protective Structures Against Fragments*

In the specific case of the demonstrator analyzed in this work, considering the input data reported in Table 5, the 3D algorithm first calculates the vulnerability of the platform, systems, and components with respect to fragments, visualizing the solutions as shown in Figure 8a,b.

Even in this case, the most critical component is the Airborne-VCR, whose vulnerability and detonation distance trend is appreciable in Figure 8b. This component will therefore serve as the component around which the optimized protection is generated.

**Table 5.** Inputs related to the 3D algorithm, specific to the considered case study.

| Input data | Description | |
|---|---|---|
| $V_m$ | Speed of the detonating object originating the fragments | 500 m/s |
| $Az_m$ | Azimuth angle of the detonating object | 180° |
| $El_m$ | Elevation angle of the detonating object | −30° |
| $DD_{min}$ | Minimum value of the detonation distance interval | 7000 mm |
| $DD_{max}$ | Maximum value of the detonation distance interval | 10,000 mm |
| $N_{DD}$ | Number of detonation distances | 6 |
| $N_{DP,xy}$ | Number of detonation points on the $x$–$y$ plane | 15 |
| $N_{DP,xz}$ | Number of detonation points on the $x$–$z$ plane | 15 |
| $P_{hi}$ | Susceptibility of the $i$-th component | 1 |
| $Height$ | Altitude of the detonation point | 500 m |
| $L_{wh}$ | Detonation object length | 381 mm |
| $D_{wh}$ | Detonation object diameter | 177.8 mm |
| $h_{wh}$ | Detonation object case thickness | 10.16 mm |
| $A_f$ | Area of the fragment | 2000 mm$^2$ |
| $m_f$ | Mass of the fragment | 0.13 kg |

As in the case of the analysis carried out for projectiles, the algorithm converges to a single solution. This particular solution presents zero vulnerability and a weight of 0.0198 (that is, 1.98% of the weight that would be achieved by fully covering the aircraft's fuselage). In Figure 9a,b, the detailed area of the platform where the protection is generated can be appreciated.

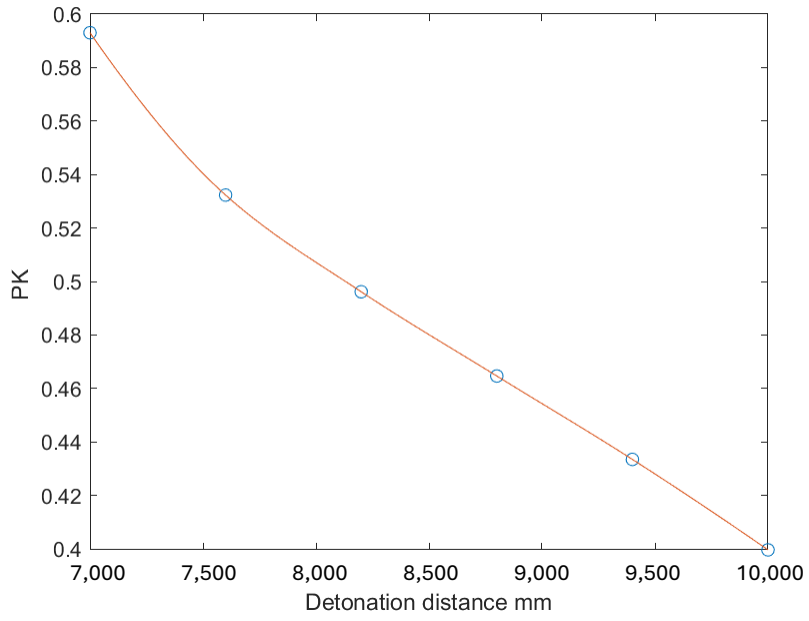


(**a**)

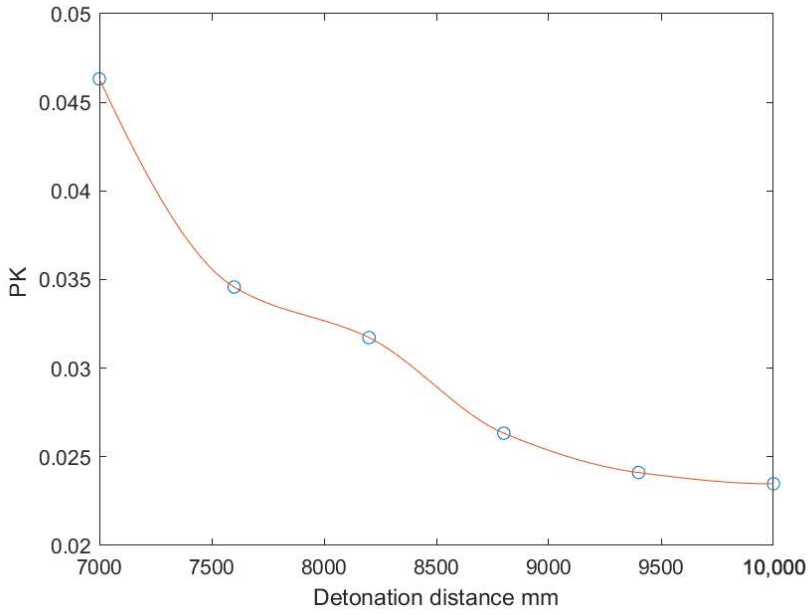


(**b**)

**Figure 8.** Vulnerability compared to the detonation distance of the entire platform (**a**) and of the most critical components (**b**).

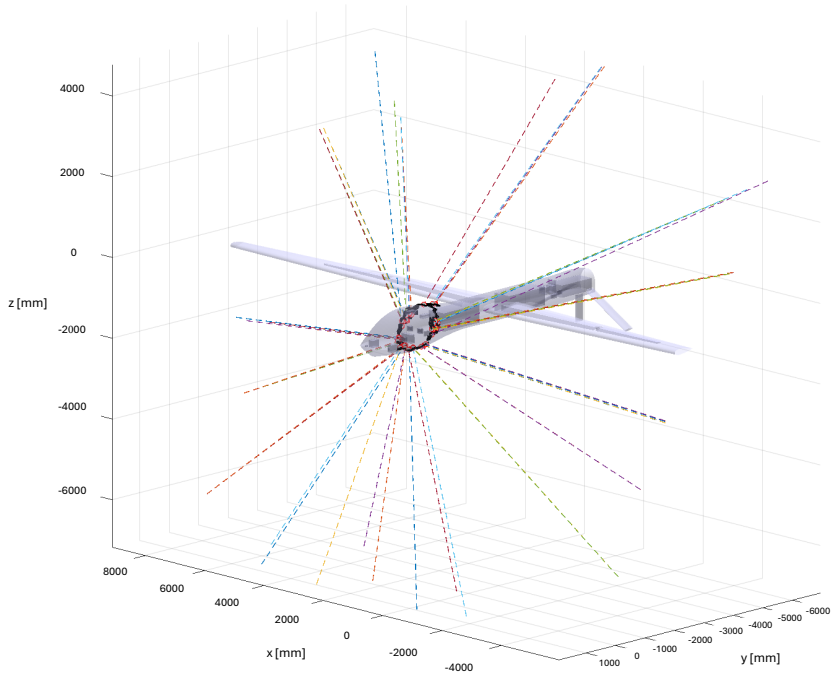


(**a**)

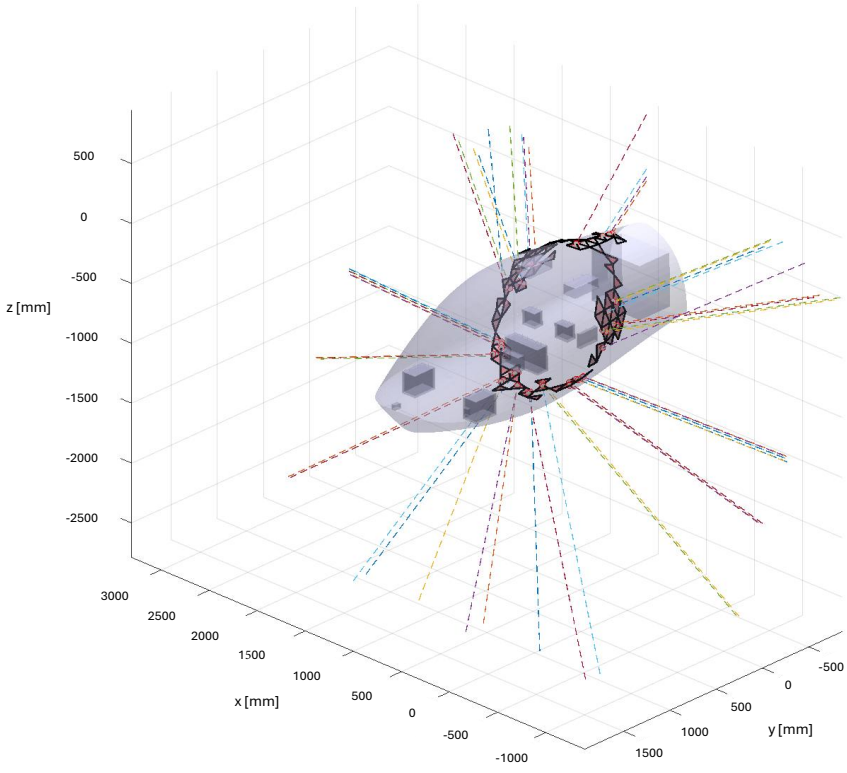


(**b**)

**Figure 9.** Optimized protection layout considering fragments as threats: (**a**) View of the platform with the integrated optimized protection. (**b**) Focus on the optimized protection shown in (**a**).

### *3.4. Estimating the Weight of Protection Versus Fragments*

Considering the impact of fragments, additional considerations can occur regarding the weight of the protection, enabling a comparison with non-optimized protections. In

particular, it is assumed that Dyneema HB26 plates are used, with the characteristics reported in Table 6.

**Table 6.** Dyneema HB26 material's characteristics [20,21].

| Dyneema HB26 | Density [kg/m$^3$] | Tension Resistance [MPa] | $E_f$ [MPa] |
|---|---|---|---|
| Plate | 970 | 3000 | 81,390 |

From Equations (4) and (5), the areal density of the fragment $AD_p$ and the target plate $AD_t$ can be determined.

$$AD_t = \rho_t \cdot t \tag{4}$$

$$AD_p = \frac{m_p}{D^2} \tag{5}$$

where $\rho_t$ represents the material density, $t$ the plate thickness, $m_p$ the mass of the fragment, and $D$ its characteristic dimension. The thickness of the plate $t$ is unknown, but, from the graph shown in Figure 10, the ratio between the areal density of the target and the fragment can be determined.

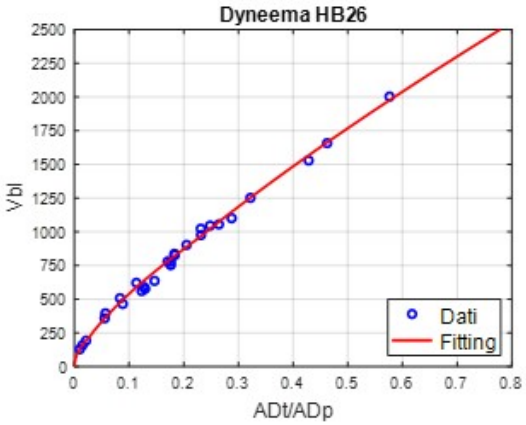


**Figure 10.** RQ-1 simplified model used as the target platform [20,21].

This ratio is calculated assuming a ballistic velocity $V_{bl}$ of 1000 m/s. As for the areal density of the fragment, this is known by assuming $D = 45$ mm and $m_p = 0.130$ kg. In this specific case, also considering Equation (6), a thickness of approximately 34 mm is obtained.

$$V_{bl} = max\left(2669.2\left(\frac{AD_t}{AD_p}\right)^{0.6957}; 1411\left(\frac{AD_t}{AD_p}\right)^{0.5192}; 3039\left(\frac{AD_t}{AD_p}\right)^{0.7825}\right) \tag{6}$$

Considering further that the surface covered by the optimized protective structures (shown in Figure 9a,b) is 409,706 mm$^2$, the volume of the protection $V_{pr}$ will be calculated as in Equation (7).

$$V_{pr} = A_{tot} \cdot t = 409{,}706 \text{ mm}^2 \cdot 34 \text{ mm} = 13{,}930{,}004 \text{ mm}^3 = 0.014 \text{ m}^3 \tag{7}$$

The value of the protective surface is calculated by summing the areas of each mesh element where the protections are placed. At this point, the weight can be calculated by multiplying the volume by the density of the considered material, obtaining a protection weight of approximately 14 kg.

## 4. Discussion

The solution to which the 2D algorithm converges, shown in Figure 7, is straightforward. In fact, to protect the target component, it covers its projection relative to the firing direction with protective material. This occurs because the case under examination is simple, with the threat coming from the front of the platform. Additionally, the grid elements where the protection is placed are very few compared to the total number of elements. As a result, the weight of the protection to which the genetic algorithm converges is very low, thus eliminating the need for even lighter solutions. In any case, the solution demonstrates that the genetic algorithm, as configured, is able to autonomously converge to a solution with minimized weight and vulnerability.

Regarding the protection to which the 3D algorithm converges, in this case, the protective structure consists of a single cluster of material, resulting in a continuous topology. This was achieved thanks to the continuity filter implemented in the code, based on graph theory.

With this protection, it is possible to conduct post-analysis evaluations on the weight. If, hypothetically, the entire external structure of the platform were covered with Dyneema HB26, instead of using optimized solutions, the additional weight to the platform structure would be far greater than the 14 kg estimated in Section 3.4, amounting to approximately 631 kg. Another solution could involve covering each component of the platform with a protective box with the same thickness as the elements of the optimized protection. In this case, the added weight to the platform would be estimated at 364 kg. In the context of aircraft, such an increase in weight is unrealistic, ruling out this type of solution.

Alternatively, if only the critical component is covered with a protective shell composed of Dyneema HB26, again with a thickness of 34 mm, a protective solution weighing 12 kg is obtained. The solution with optimized topology, therefore, is slightly heavier but, being positioned on the fuselage, offers partial protection to other components near the target component.

Finally, considering the possibility of adopting a regular circular-ring-shaped protective solution, again on the fuselage and around the critical component, with the same thickness, a protection weighing 15 kg is obtained. Adopting the optimized protection, therefore, enables saving about 7% in weight compared to the ring-shaped solution. Moreover, the same circular ring is based on an area that follows the optimized solution, itself derived from the optimization process, and could represent the engineering solution.

## 5. Conclusions

In this work, a vulnerability analysis was conducted on RPAS systems using a specifically designed computational environment. The methodologies for correctly modeling the 3D models of critical components were discussed, and the data required to perform the analysis using the software modules were identified. These procedures were applied to a representative case study, and the results obtained from the vulnerability analysis were subsequently reported. This phase enabled a concrete evaluation of the applicability of the developed software, providing a practical view of its effectiveness. Considering the results obtained from the vulnerability analysis, the component identified as the most critical, both with respect to projectiles and fragments, was the Airborne-VCR. This component is part of the system that is responsible for connecting and facilitating communication between the platform and the ground unit. Consequently, the software selects this component to generate optimized protections, considering threats from both fragments and impacting objects. The protection generation and optimization module produced structures that eliminate the vulnerability of the identified critical component, converging toward continuous solutions that lead to a significant weight reduction compared to non-optimized protections. The analysis of the results, in general, revealed a consistent correspondence with the theory

used for software programming. This aspect highlights the robustness and reliability of the adopted methodology, confirming its ability to identify and assess platform vulnerabilities and subsequently generate optimized protective solutions. The computational times of the software for each module are manageable. Despite the complexity of the analyzed demonstrator, the execution times of the modules range from minutes to hours.

**Author Contributions:** Conceptualization, S.A., L.L. and A.M.; methodology, S.A. and L.L.; software, S.A. and L.L.; validation, S.A.; formal analysis, S.A. and L.L.; investigation, S.A. and L.L.; resources, S.A.; data curation, S.A.; writing—original draft preparation, S.A.; writing—review and editing, S.A., L.L. and A.M.; visualization, S.A.; supervision, A.M.; project administration, A.M.; funding acquisition, A.M. and M.G. All authors have read and agreed to the published version of the manuscript.

**Funding:** This research received no external funding.

**Institutional Review Board Statement:** Not applicable.

**Informed Consent Statement:** Not applicable.

**Data Availability Statement:** The data related to the components listed in Table 3 are freely available online at the following links: https://www.oxts.com (accessed on 10 May 2024); https://chelton.com/media/smhen3k1/chelton-antenna-catalogue-2022-web.pdf (accessed on 10 May 2024); https://www.activesilicon.com/products/harrier-10x-af-zoom-camera/ (accessed on 10 May 2024); https://store.ctr-electronics.com/power-distribution-panel/ (accessed on 10 May 2024); https://www.ebay.it/itm/324436149310?mkevt=1&mkcid=1&mkrid=724-53478-192550&campid=5338954104&toolid=20006&customid=5c3f96bf1ca453ed75bbf05336385dae (accessed on 10 May 2024); https://www.volz-servos.com/actuators/detail/da-30-ht-d/ (accessed on 10 May 2024); https://www.raybuck.com (accessed on 10 May 2024); https://sterling-power.com/collections/alternator-regulators/products/universal-advanced-digital-alternator-regulator-pro-reg-dw-waterproof (accessed on 10 May 2024); https://flyrotax.com (accessed on 10 May 2024); https://www.improvedracing.com/setrab-19-row-series-6-oil-cooler.html. (accessed on 10 May 2024).

**Conflicts of Interest:** The authors declare no conflicts of interest.

## References

1. Ball, R.E. *The Fundamentals of Aircraft Combat Survivability: Analysis and Design*; AIAA Education Series; AIAA: Reston, VA, USA, 1985.
2. Kopp, C. Are helicopters vulnerable? *Aust. Aviat.* **2005**, *59*, 59–63.
3. Arrighi, J.A. Survivability design features incorporated in the A-10: A close Air support weapon system. In Proceedings of the Third Biennial Aircraft Survivability Symposium, Monterey, CA, USA, 30 October–2 November 1978.
4. Vice, J.M. Survivability/vulnerability information analysis center (SURVIAC): A tool for the aircraft survivability community. *J. Aircr.* **1987**, *24*, 511–515. [CrossRef]
5. Aitken, E.D.; Jones, S.L.; Dean, A.W. *A Guide to FASTGEN Target Geometric Modeling*; US Army Research Laboratory: Users Manual; ASI Systems International: Fort Walton Beach, FL, USA, 1993.
6. Pei, Y.; Wang, W.; Li, L. Ranking the vulnerable components of aircraft by considering performance degradations. *J. Aircr.* **2016**, *53*, 1400–1410. [CrossRef]
7. Pei, Y.; Cheng, T. Importance measure method for ranking the aircraft component vulnerability. *J. Aircr.* **2014**, *51*, 273–279. [CrossRef]
8. Kincheloe, W.; Edwards, E.; Klopcic, J.T.; Walbert, J.; Deitz, P.; Reed, H., Jr.; Hacker, W.; Bely, D. *Fundamentals of Ground Combat System Ballistic Vulnerability/Lethality*; American Institute of Aeronautics and Astronautics, Inc.: Reston, VA, USA, 2009.
9. Yoo, C.; Park, K.; Choi, S.Y. The vulnerability assessment of ground combat vehicles using target functional modeling and FTA. *Int. J. Precis. Eng. Manuf.* **2016**, *17*, 651–658. [CrossRef]
10. Brownlow, L.C.; Goodrum, C.J.; Sypniewski, M.J.; Coller, J.A.; Singer, D.J. A multilayer network approach to vulnerability assessment for early-stage naval ship design programs. *Ocean. Eng.* **2021**, *225*, 108731. [CrossRef]
11. Kane, C.; Schoenauer, M. Topological optimum design using Genetic Algorithms. *Control Cybern.* **1996**, *25*, 1059–1088.
12. Holland, J. *Adaptation in Natural and Artificial Systems*; MIT Press: Boston, MA, USA, 1975.
13. Goldberg, D. Genetic Algorithms in Search, Optimization and Machine Learning. *Addion Wesley* **1989**, *1989*, 36.

14. Sigmund, O. Materials with prescribed constitutive parameters: An inverse homogenization problem. *Int. J. Solids Struct.* **1994**, *31*, 2313–2329. [CrossRef]
15. Sigmund, O. On the design of compliant mechanisms using topology optimization. *J. Struct. Mech.* **1997**, *25*, 495–526. [CrossRef]
16. Xie, Y.M.; Steven, G.P. A simple evolutionary procedure for structural optimization. *Comput. Struct.* **1993**, *49*, 885–896. [CrossRef]
17. Xie, Y.M.; Steven, G.P. *Evolutionary Structural Optimization*; Basic evolutionary structural optimization; Springer: London, UK, 1997; pp. 12–29.
18. Lomazzi, L.; Cadini, F.; Giglio, M.; Manes, A. Vulnerability assessment to projectiles: Approach definition and application to helicopter platforms. *Def. Technol.* **2022**, *18*, 1523–1537. [CrossRef]
19. Annunziata, S.; Lomazzi, L.; Giglio, M.; Manes, A. Topological optimization of ballistic protective structures through genetic algorithms in a vulnerability-driven environment. *Def. Technol.* **2024**, *40*, 125–137. [CrossRef]
20. Iannucci, L.; Del Rosso, S.; Curtis, P.T.; Pope, D.J.; Duke, P.W. Understanding the thickness effect on the tensile strength property of Dyneema® HB26 laminates. *Materials* **2018**, *11*, 1431. [CrossRef] [PubMed]
21. Chricker, R.; Mustacchi, S.; Massarwa, E.; Eliasi, R.; Aboudi, J.; Haj-Ali, R. Ballistic penetration analysis of soft laminated composites using sublaminate mesoscale modeling. *J. Compos. Sci.* **2021**, *5*, 21. [CrossRef]